Microscopy and rock magnetism of fine grain-size titanomagnetite from the Jacupiranga Alkaline Complex, Brazil: unearthing Ti-magnesioferrite nanoparticles

Luis M. Alva-Valdivia*, María de la Luz Rivas-Sánchez, Jesús Arenas-Alatorre, Avto Goguitchaishvili and Omar Ferreira Lopes

Resumen

Se seleccionaron muestras muy finas de zonas mineralizadas del complejo Jacupiranga de la mina Cajatí para efectuar la identificación cristalográfica de nanoestructuras de titano-magnesioferrita (TMf) embebidas en titanomagnetita (TM) usando microscopía de transmisión de alta resolución (TEM). Se redujo un concentrado magnético a partir de muestras de piroxenita (sitios 4 a 7), después se dividió en fracciones de rangos de tamaño distintos: 26±2 µm, 19±1 µm, 13±1 µm, 9±1 µm, 6±1 µm and 6–0.1 µm. Las muestras mineralizadas de piroxenita y carbonatita se caracterizaron por: difracción de rayos-X, microscopía de luz transmitida y reflejada, y microscopía electrónica de barrido con análisis multielemental. La muestra de concentrado más fino (MC_6) se analizó por microscopía TEM y campo anular obscuro de ángulo alto y espectroscopía Ramán.

Se midieron las propiedades magnéticas de las distintas fracciones granulométricas, mostrando cambios drásticos cuando los tamaños de grano pasan de tamaños micro a nanométricos. El porcentaje de susceptibilidad magnética dependiente de la frecuencia ($\chi_{fd\%}$) arrojó valores altos (10.2%) para las fracciones más finas (6±1 µm y 6–0.1 µm), lo que se atribuyó a las fracciones dominantes de partículas superparamagnéticas. Los tamaños de grano nanométrico y < 6 µm de TMf en partículas de TM requirió de un campo magnético de hasta 249 mT para alcanzar la saturación durante los experimentos de magnetización remanente isotermal. La coercitividad y la magnetización remanente de esas muestras aumentaron cuando los tamaños de las partículas disminuían, probablemente debido a efectos de acoplamiento paralelo. Los experimentos de susceptibilidad magnética versus calentamientos se efectuaron dos veces en la misma muestra (<35 nm), mostrando que la repetibilidad durante el segundo calentamiento se debe probablemente a la formación de nuevas nanopartículas de TMf, y al crecimiento de las ya existentes durante el proceso del primer calentamiento.

Palabras clave: nanopartículas de titanomagnesio-ferrita, propiedades magnéticas, mineralogía, efecto del tamaño de grano, complejo alcalino Jacupiranga, Brasil.

L.M. Alva-Valdivia*
M.L. Rivas-Sánchez
Laboratorio de Paleomagnetismo
Instituto de Geofísica
Universidad Nacional Autónoma de México
Ciudad Universitaria, 04510
México DF, México
*Corresponding author: lalva@geofisica.unam.mx

J. Arenas-Alatorre
Departamento de Materia Condensada
Instituto de Física
Universidad Nacional Autónoma de México
Ciudad Universitaria, 04510
México DF, México

A. Goguitchaishvili
Laboratorio Interinstitucional de Magnetismo Natural
Instituto de Geofísica
Universidad Nacional Autónoma de México
Campus Morelia, Michoacán, México

O. Ferreira Lopes
Universidade Federal do Paraná
Departamento de Geologia
Jardim das Américas
Curitiba, Paraná, Brazil

L.M. Alva-Valdivia, M.L. Rivas-Sánchez, J. Arenas-Alatorre, A. Goguitchaishvili and O. Ferreira Lopes

Abstract

Very fine samples from the mineralized zones of the Jacupiranga complex at the Cajatí mine were selected for crystallographic identification of Ti-magnesioferrite (TMf) nanostructures embedded in titanomagnetite (TM) using high-resolution transmission electron microscopy (TEM). A magnetic concentrate obtained of pyroxenite samples (sites 4 to 7) was reduced and divided into fractions of distinct range sizes: 26±2 μm, 19±1 μm, 13±1 μm, 9±1 μm, 6±1 μm and 6−0.1 μm. The mineralized samples of carbonatite and pyroxenite were characterized by X-ray diffraction, transmitted and reflected light microscope, and scanning electron microscope with multielemental analysis. The finest magnetic concentrate sample (MC_6) was analyzed under high-resolution transmitted electron microscopy (TEM) and high angle annular dark field and Raman spectroscopy. Magnetic properties were measured for the distinct granulometric fractions, showing drastic changes when grain sizes go beyond the frontier from micro to nanometer sizes. Frequency-dependent magnetic susceptibility percentage ($\chi_{fd\%}$) report higher values (10.2%) for the finer fractions (6±1 μm and 6−0.1 μm) attributed to dominant fractions of superparamagnetic particles. Nanometer and < 6 μm grain size TMf in TM particles require a magnetic field up to 249 mT to reach saturation during the isothermal remanent magnetization experiment. Coercivity and remanent magnetization of these samples increase when the particle size decreases, probably due to parallel coupling effects. Magnetic susceptibility versus temperature experiments were conducted two times on the same (< 35 nm) sample, showing that the repetition during the second heating is probably due to the formation of new TMf nanoparticles and growth of those already present during the first heating process.

Key words: TMf nanoparticles, magnetic properties, mineralogy, grain size effect, Jacupiranga Alkaline Complex, Brazil.

Introduction

The ubiquity of tiny particles of minerals -mineral nanoparticles- in mineral deposits, oceans and rivers, atmosphere and soils are providing scientists with new ways of understanding Earth's processes. Our planet's physical, chemical, and biological processes are influenced or driven by the properties of these minerals. The way in which these infinitesimally small minerals influence Earth's systems is more complex than previously thought (Hochella *et al*., 2008).

Minerals have an enormous range of physical and chemical properties due to a wide range of composition and structure, including particle size. Nanominerals, however, have one critical difference: a range of physical and chemical properties, depending on their size and shape. This difference changes our view of the diversity and complexity of minerals, and how they influence Earth systems (Hochella, 2008).

Nanoscale structures are critical in determining the magnetic properties of minerals. Harrison (2007) describes that the fundamental importance of magnetism at this length scale has been overlooked in the past, leaving a number of long-standing paleomagnetic and rock-magnetic observations that could not be explained (Feinberg *et al*., 2007). Examples include the origin of strong and stable magnetic anomalies on Mars and the phenomenon of self-reversed thermoremanent magnetization (McEnroe *et al*., 2004). This gap in understanding arose because the technology required to study mineral magnetism with nanometer resolution had not been developed. We have now begun to establish quantitative links between the nanoscale structure of natural magnetic minerals and their macroscopic magnetic properties (Harrison, 2007).

For this study, we used the paleomagnetic samples from eight sites of the Jacupiranga alkaline-carbonatitic complex, Cajati mine, located at the southeastern region of Brazil (48°09'W, 24°41'S). The carbonatite belongs to the Jacupiranga Ultramafic Alkaline Complex of Early Cretaceous age (131 Ma, Ruberti *et al*., 2000). This Complex has an oval shape in a regional map showing Brazil and the study area (Figure 1).

One of its silicate rocks is widely known as "jacupirangite". Among carbonatitic phases, there are different compositions (calciocarbonatites to magnesiumcarbonatites) forming independent plugs, dykes and dyke swarms. The main mineralized geological setting can be recognized as formed by carbonatitic portions (both of calcic and dolomitic composition) separated by specific features as well as other lithological ore types, like minor portions of phoscoritic composition.

The aim of this study is to report the unearthing of TMf nanoparticles embedded in TM (finest magnetic concentrate) by crystallographic analysis of nanostructures using high-resolution TEM, and to determine the effect on the rock magnetic properties of its grain-size, and its influence on the origin and deposition environment.

Experimental methods and sample description

The eight paleomagnetic rock sampled sites (described in detail by Alva-Valdivia *et al*., 2009) are as follows: Site 1, coarse grain carbonatite;
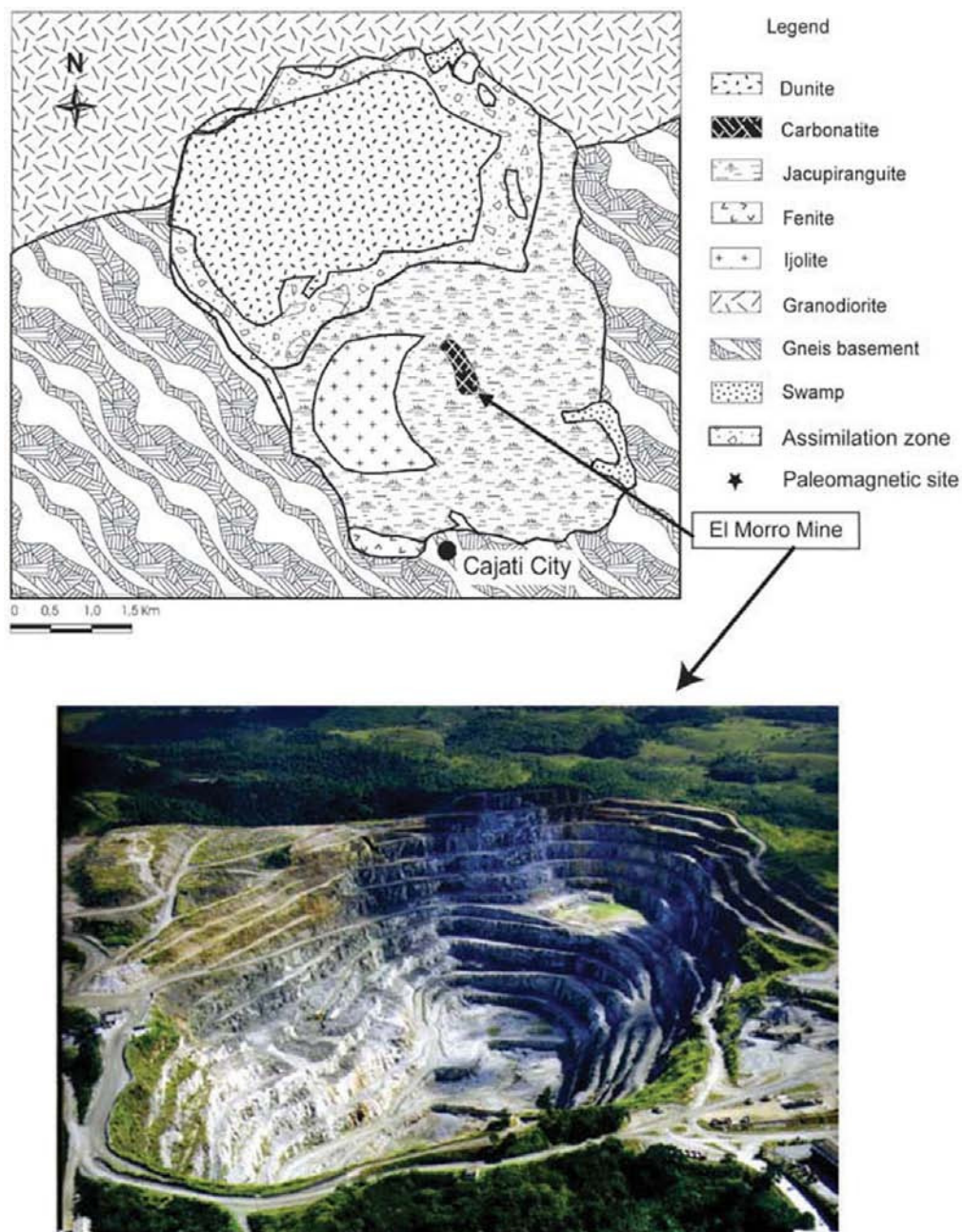
Figure 1. Location of the study area: precise location of sampled sites is in figure 1 of Alva-Valdivia *et al*. (2009).

Site 2, medium grain carbonatite; Site 3, fine grain carbonatite; Site 4, 5 and 6, pyroxenite Jacu-piranga; Site 7, carbonatite- pyroxenite contact; and Site 8, granodiorite intrusive.

We select one paleomagnetic standard rock specimen (1" diameter and 2.2 cm long) from each pyroxenite site (4 to 7). Then all of the four samples were crushed together and put in a magnetic separator to get a magnetic concentrate of different grain-size fractions using the "hydro-cycle method" (Rivas-Sánchez *et al*., 2009 describe in detail the equipment and crushing processes). Each specific size fraction was prepared with an average variation around one micron. Granulometric fractions are: MC_1 (26 ± 2 μm); MC_2 (19 ± 1 μm); MC_3 (13 ± 1 μm); MC_4 (9 ± 1 μm); MC_5 (6 ± 1 μm); and MC_6 (6 ~ 0.1 μm). These size fractions and the sample containing TMf nanoparticles (MC_6) were characterized according to their crystalline, physicochemical and magnetic properties.

Transmitted and reflected light microscopy study was done with a Leica DM-LP model; for X-ray diffraction (XRD) we used a Geiger-Flex model Rigaku difractometer, setting in an aluminum sample-holder of a non-oriented fraction, in the angular interval 2θ of 4° to 80° at two distinct velocities (1/2° by minute and 1° by minute); electron probe X-ray micro-analyzer (EPMA) JEOL, JXA 8900-R for multi-elemental analyses via WDS; Raman spectrometry was achieved by using a source of monochromatic infrared laser irradiation (dispersed radiation by molecules at a fixed angle was registered); and high-resolution TEM with a JEOL 2010 FEG FASTEM.

Magnetic susceptibility at varying frequencies was measured by using a Bartington Instruments MS2 linked to a MS2B dual frequency sensor. We used low frequency (χ_{lf} = 470 Hz) and high frequency (χ_{hf} = 4700 Hz) to detect qualitatively the presence of ultrafine grain size carriers of superparamagnetic (SP) behavior. The magnetic susceptibility as a function of temperature was determined by means of a Bartington MS2 susceptibilimeter, with a MS2W sensor coupled to a MS2WFP furnace. To measure the hysteresis parameters and isothermal remanent magnetization (IRM) acquisition and backfield demagnetization curves, we used an alternating field-force gradient magnetometer, Micromag 2900.

Results
Mineralogy and microscope analyses
Optical Microscopy

Alva-Valdivia *et al*. (2009) report petrography of the rock units, which have been studied again in order to look for details in the oxide minerals (Fe and Fe-Ti) and choose micro-areas with high probability of nanoparticle mineral occurrence.

At least one polished section from each site was studied by optical microscopy and EPMA in order to determine the composition and mineral textural relationships, which was later verified by XRD and Raman spectroscopy, as follows:

1) Carbonatites show an alotriomorphic granular mosaic of grain size ranging from 300 to 7,000 µm, formed mainly by non-metallic minerals of the carbonate group, as: calcite, dolomite and aragonite, all associated to apatite with minor amount of olivine (forsterite), phlogopite, pectolite, zircon and zirkelite. The metallic minerals are present in minor proportion and correspond to: magnetite, titanomagnesioferrite, scarce geikielite and sulfides (pyrite, pyrrothite and marcasite), filling open spaces between the primary minerals.

2) The pyroxenites have coarse-granular grain texture (220 to 1000 µm), composed mainly by non-metallic minerals: hedenbergite, diopside, and less apatite, Fe-Mg spinel and scarce quartz. The metallic minerals are: titanomagnetite, ilmenite, magnesioferrite, titanomaghemite (TMg) and titanohematite (TH), in minor proportion. These metallic minerals are filling open spaces in the host rock. Massive TM range in grain size from 380 µm to 6000 µm, with approximately 12% of Ti content slightly altered to TH, observed with graphic and lamellar intergrowths of ilmenite and ferrian spinel in a trellis type texture (Figure 2).
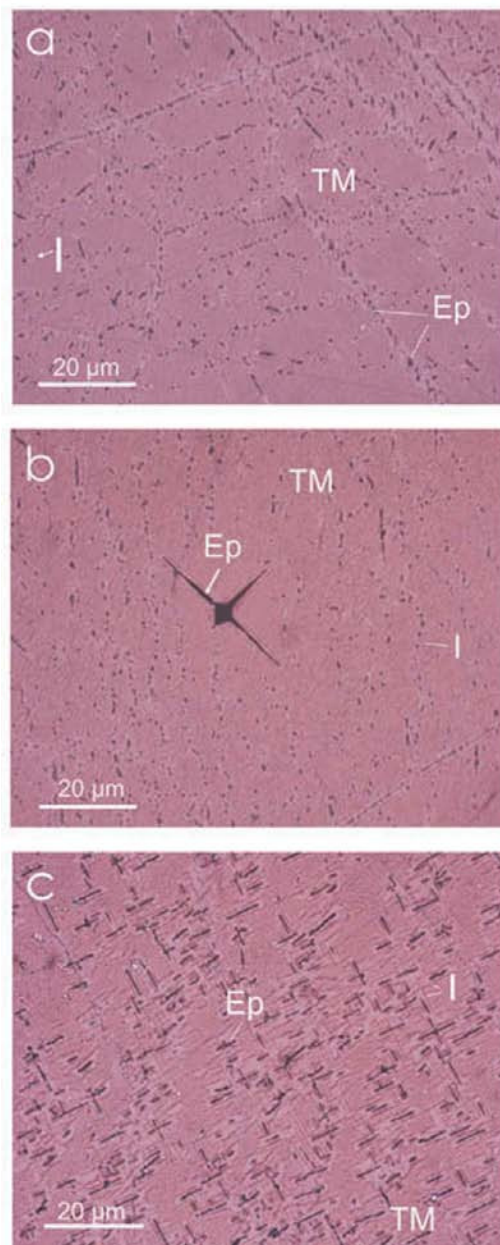

Figure 2. Representative photomicrographs of TM in pyroxenites using parallel nichols and reflected light. (a) ilmenite exsolutions (I) and Fe spinel (Ep); (b) ilmenite exsolutions and acicular shape of Fe spinel; and (c) exsolved ilmenite lamellas and Fe spinel.

3) Alva-Valdivia *et al*. (2009) confirmed the effect of hydrothermal processes in both rock types, as indicated by the next factors: a) In the carbonatite, the magnetite is massive and because of their relationship with rock forming mineral, suggests post-crystallization in relation to these minerals maybe during the latest phase of magmatic differentiation (possibly a high-temperature hydrothermal phase); b) In the pyroxenite, the TM form an altered metasomatic texture with pyroxene grains, suggesting the effect of hydrothermal processes of primary mineralization produced by the intrusive rock. They also report the presence of ionic exchange, Fe^{2+} by Mg in the mineralization of both rock types. In the carbonatite, they did not distinguish Ti in the selected micro-zones of magnetite and magnesioferrite, contrasting with the pyroxenite samples that show up to 10% of Ti in both titanomagnetite and magnesioferrite.

Summarizing, the petrographic characterization of the Jacupiranga complex, define two rock hosts type: carbonatite and pyroxenite. In these both rock types, Fe oxide minerals (magnetite and TM, respectively) are affected in its crystalline structure by partial substitution of Fe^{+2} by Mg, with formation to magnesioferrite. Being conspicuous the Ti enrichment of oxide mineral (Fe and Fe-Mg) of the pyroxenite. Optical microscopy shows a non-usual roughly texture of the TM with abundant ilmenite emulsion-type exsolution, magnesioferrite and Fe-spinel slightly detected at high amplification. Most of the exsolution measured are below 0.1 μm.

Mineral chemistry

Table 1 show results of mineral chemistry and structural formula of oxide minerals (Fe and Fe-Ti) identified in the carbonatite and pyroxenite. The quantitative chemical analyses were done by EPMA. In the carbonatite, the oxide minerals correspond to magnetite and magnesioferrite. In the pyroxenite, oxides show particular chemical characteristics in its structural formula, being conspicuous the TiO_2 presence. We named TM and TMf, with a structural formula of Ti content up to 12 and 14%, respectively. The Fe-Ti oxide corresponds to ilmenite.

In both rock types (carbonatite and pyroxenite), the oxide minerals are replaced by geikielite, and partial ion substitution of Fe^{+2} by Mg was observed, while geikielite is enriched in Fe.

X-ray diffraction (XRD)

To verify the occurrence of magnesioferrite, maghemite and hematite in the pyroxenite and ultramafic rocks, we used XRD, these minerals have an important amount of Ti, which was confirmed by the multielemental analyses of EPMA results via WDS. Because of the Ti presence, we add the prefix 'titano' to the minerals, changing to TMf, TMg and TH.

A mineralogical characterization by XRD analyses was done in an original natural sample (Table 2) that confirmed the magnesioferrite, maghemite and hematite presence. Figure 3a, and 3b shows well-defined peaks in the XRD spectra.
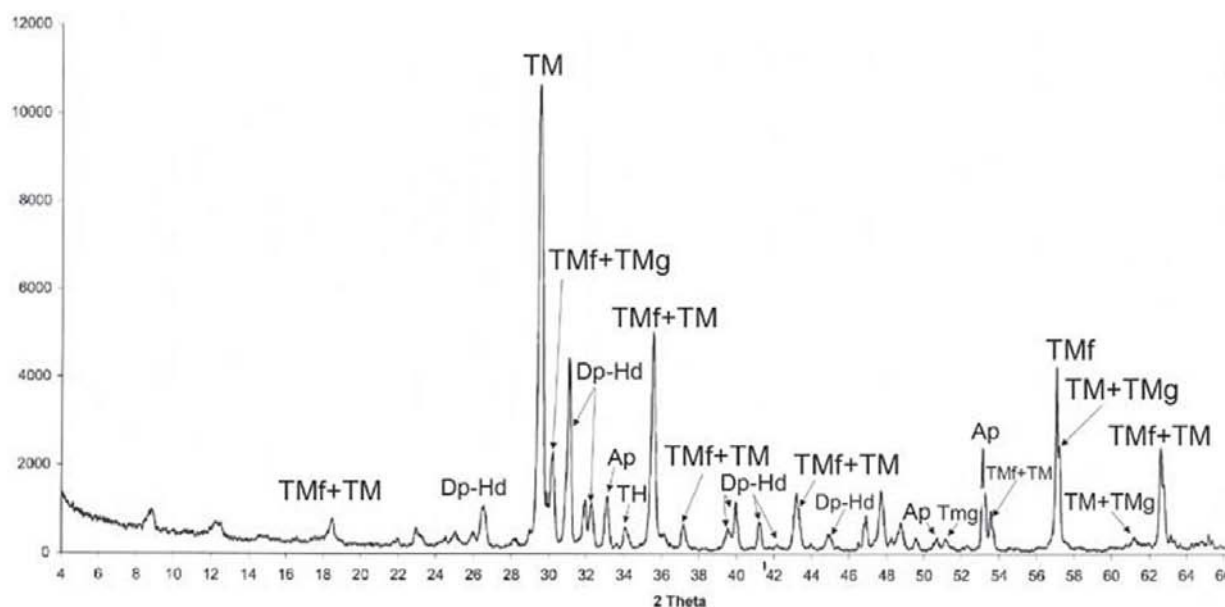

Figure 3a. XRD spectrum of the pyroxenite (Jacupiranga). TM, Ti-magnetite; TMf, Ti-magnesioferrite; TMg, Ti-maghemite; TH, titanohematite; Dp, diopside-hedenbergite; Ap, apatite.

Table 1. Mineral chemistry and structural formula of Fe oxides in pyroxenite.

Oxides and ions	1 Magnetite	2 Magnetite	3 Magnetite	4 Magnesio-ferrite	5 Magnesio-ferrite	6 Geikielite	7 Geikielite	8 Geikielite
Fe_2O_3	61.403	65.402	65.827	87.252	77.266	---	---	---
FeO	27.696	29.499	29.691	---	---	27.404	27.893	23.773
TiO_2	2.881	2.934	---	1.163	1.656	54.997	55.373	58.228
MnO	0.612	---	0.012	---	1.061	2.592	4.764	5.173
MgO	3.829	1.731	1.452	8.367	9.926	9.039	7.349	8.043
CaO	---	0.024	----	0.779	0.329	0.352	0.074	0.310
Cr_2O_3	---	0.349	0.332	---	---	---	1.417	---
NiO	0.636	---	0.936	0.738	0.986	2.129	---	1.451
SiO_2	0.459	---	0.209	0.819	0.626	0.885	---	0.379
Al_2O_3	---	---	0.186	0.734	1.933	---	---	---
Na_2O	2.044	---	0.073	0.327	3.897	---	---	0.705
K_2O	---	---	---	---	---	---	---	---
Σ	99.56	99.939	98.718	100.179	97.680	97.398	96.870	98.062
Fe^{+3}	13.891	14.868	15.349	17.899	16.180	---	---	---
Fe^{+2}	6.963	7.453	7.694	---	---	1.106	1.133	0.941
Ti	0.651	0.667	---	0.238	0.347	1.997	2.023	2.073
Mn	0.156	---	0.003	---	0.250	0.106	0.196	0.207
Mg	1.716	0.779	0.671	3.399	4.116	0.653	0.532	0.567
Ca	---	0.008	---	0.227	0.098	0.018	0.004	0.016
Cr	---	0.083	0.081	---	---	---	0.054	---
Ni	0.154	---	0.233	0.162	0.221	0.083	---	0.055
Si	0.138	---	0.065	0.223	0.174	0.226	---	0.096
Al	---	---	0.068	0.236	0.634	---	---	---
Na	1.191	---	0.044	0.173	2.103	---	---	0.065
K	---	---	---	---	---	---	---	---
Σ	24.861	23.858	24.208	25.557	24.123	4.189	3.942	4.020

Oxides and ions	9 Titano-magnetite	10 Titano-magnetite	11 Titano-magnetite	12 Titano-magnetite	13 Titano-mag-nesioferrite	14 Ilmenite	15 Geikielite	16 Geikielite
Fe_2O_3	52.018	54.403	53.229	54.797	72.253	---	---	---
FeO	23.462	24.583	24.009	23.916	---	42.439	25.812	24.468
TiO_2	12.182	12.917	13.007	12.920	14.839	42.424	60.620	60.905
MnO	1.626	1.127	0.486	0.885	0.695	0.252	0.366	1.288
MgO	3.554	3.352	3.589	3.174	5.086	9.638	11.542	10.357
CaO	---	0.401	0.190	---	0.426	0.374	0.034	0.618
Cr_2O_3	0.489	0.447	0.491	0.241	---	1.707	0.496	0.468
NiO	0.680	---	0.749	0.576	0.400	---	---	---
CoO	2.485	0.086	1.716	0.299	1.076	1.432	0.095	---
V_2O_3	---	---	0.425	0.023	---	0.253	---	0.576
SiO_2	0.395	---	0.125	0.450	0.215	---	---	---
Al_2O_3	2.428	2.453	2.188	2.450	4.925	1.203	0.207	0.232
Na_2O	0.483	0.395	0.212	0.073	---	0.280	0.714	0.184
K_2O	---	---	---	---	---	---	---	---
Σ	99.802	100.164	100.416	99.804	99.915	100.002	99.886	99.096
Fe^{+3}	11.184	11.584	11.315	11.667	14.166	---	---	---
Fe^{+2}	5.606	5.817	5.672	5.659	---	1.770	0.981	0.935
Ti	2.617	2.748	2.763	2.749	2.908	1.592	2.072	2.092
Mn	0.393	0.270	0.116	0.212	0.153	0.010	0.014	0.049
Mg	1.513	1.413	1.511	1.338	1.975	0.717	0.782	0.705
Ca	---	0.121	0.058	---	0.118	0.020	0.002	0.030
Cr	0.110	0.099	0.109	0.054	---	0.067	0.018	0.017
Ni	0.156	---	0.170	0.131	0.084	---	---	---
Co	0.569	0.019	0.388	0.067	0.225	0.057	0.004	---
V	---	---	0.079	0.004	---	0.008	---	0´017
Si	0.113	---	0.035	0.127	0.056	---	---	---
Al	0.818	0.818	0.729	0.817	1.513	0.071	0.011	0.013
Na	0.268	0.217	0.116	0.040	---	0.070	0.063	0.016
K	---	---	---	---	---	---	---	---
Σ	23.347	23.106	23.061	22.865	21.198	4.382	3.947	3.857

CARBONATITE:
1, 2, 3 Euhedral magnetite. Site 1
4, 5 Massive magnesioferrite. Site 1
6, 7, 8 Magnetite and magnesioferrite surrounded by geikielite, also filling open spaces between these minerals.

PIROXENITE JACUPIRANGA:
9, 10, 11, 12 Massive titanomagnetite
13 Titanomagnesioferrite exsolution in titanomagnetite
14 Ilmenite emulsion type exsolutions in the titanomagnetite
15, 16, 17 Geiquielite surrounding titanomagnetite and filling open spaces in this.

Figure 3b. The sample was annealed at 350°C, and the residual material was analyzed by XRD. The diffraction spectra pattern (and structure) of Ti-maghemite increase with temperature.
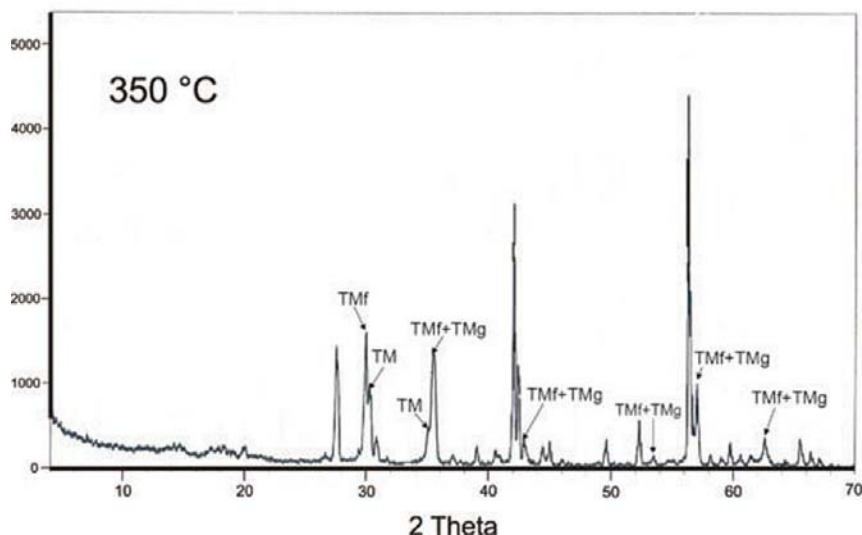

Table 2. XRD results.

Sample	Mineral phase
Pyroxenite Jacupiranga	Magnetite: Fe_3O_4 [19-629] Magnesioferrite: $MgFe_2O_4$ [36-0396] Pyroxene group: diopside-hedenbergite: $Ca(Mg, Fe)$ $[Si_2O_6]$[11-654, 25-160] Apatite: $CaF(Po_4)3$ [15-876] Maghemite: $\gamma\text{-}Fe_2O_3$ [4-0755] Hematite: $\alpha\text{-}Fe_2O_3$ [89-0599]

Also, we got the mineral chemistry composition of the iron oxides identified in the carbonatite and pyroxenite host rocks, respectively, Table 1 (1 - 5 and 9 - 13).

Raman spectroscopy

We studied six samples of sites MC_4 and MC_5 corresponding to the ultramafic rocks (pyroxenite). Fine to ultrafine size of ilmenite disseminated in TM was identified by optical microscopy, showing exsolution emulsion-type shape. Figure 4 shows some Raman spectra examples of ilmenite from the Jacupiranga pyroxenite. These spectra show three distinctive peaks (ilmenite Raman), which appear at 220, 398 and 680 cm^{-1}, confirming that ilmenite is certainly present in this rock.

Raman spectra of selected regions of TM are shown in Figure 5. Magnetite is clearly identified by three peaks slightly moved regarding their wavenumber (cm^{-1}) due to the Ti presence. This spectra support the presence of TM with a content of TiO_2 up to 12%. We show the first TM Raman analysis, which allowed to establish their structural

characteristics and assert their classification (chemical composition was determined by WDS).

High resolution TEM

TMf nanoparticles and likely ilmenite nanoparticles were identified in samples corresponding to the ultrabasic (pyroxenite) rocks. Nanoparticles are 5 to 10 nm size.

The crystallographic analysis of TMf structures was made with the purpose to determine the structural characteristics and assert its classification. We obtained (Figure 6) dark and clear (bottom) field high resolution and Fast Fourier Transform (FFT) (upper right) images by using the high resolution TEM. Each mineral nanostructure was crystallographically studied, measuring interplanar distances and getting their diffraction patterns.

TMf of nanometer scale was identified oriented along the edge [1 1 2] with interplanar distances $d_1 = 2.98$ Å, $d_2 = 1.48$ Å that correspond to the planes (220) and (311), respectively (Figure 6).
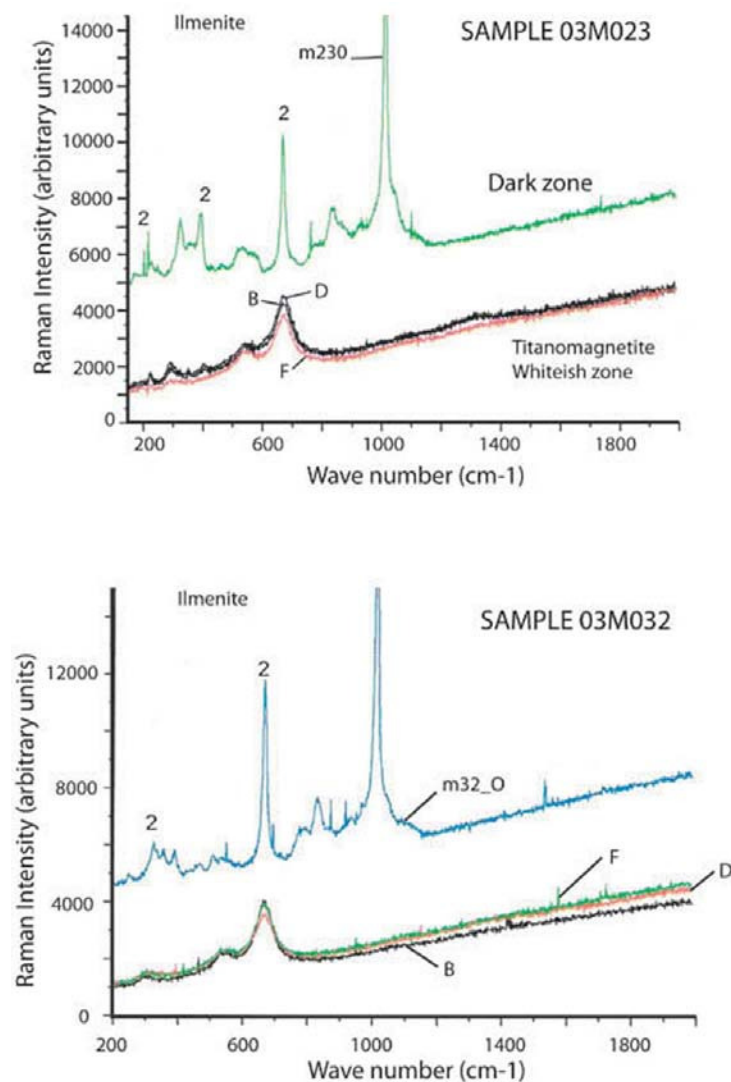
Figure 4. Raman spectra of selected regions indicating ilmenite from samples 03M023 and 03M032.

The possible ilmenite is oriented along the edge [1 0 4] with interplanar distances $d_1 = 2.72$ Å, $d_2 = 2.52$ Å that correspond to the planes (104) and (110), respectively, unfortunately was not possible to get a clear image of this mineral.

Rock and mineral magnetic properties of the pyroxenite

Frequency-dependent magnetic susceptibility percentage ($\chi_{fd\%}$).

We used a very small amount of natural material (magnetic concentrate) in order to avoid saturation of equipment and to reach better uniformity of the sample during the measurement. Carbonatites were not used for this experiment because they did not show any evidence (optical microscopy) of nanoparticles presence. The selected-analyzed samples by this technique correspond to TM and TMf with size range from 26

µm up to 0.1 µm (MC_1, MC_2, MC_3, MC_4, MC_5 and MC_6) (Table 3). We used the model proposed by Dearing *et al*. (1996) using theoretical predictions and data from synthetic grains and environmental samples, to suggest an interpretation of our results of frequency-dependent magnetic susceptibility: $\chi_{fd\%} < 5$ in TM samples of 0.2 to 7 µm grain size are attributed to grains formed by the union of (assemblages) extremely fine particles (< 5 nm), together with the mineral concentration and grain size distribution; TM grain size of 0.1 µm to 26 µm range were identified with abundant inclusions of TMf nanoparticles; the fraction between 9 and 26 µm report low values of $\chi_{fd\%} < 5$ attributed to the micro-nanometer textural association that mask the SP signal; finally, we obtained high values of $\chi_{fd\%}$ (9.6 and 10.2) for the fractions ranging from 0.1 to 6 µm, respectively (samples MC5 and MC6, Table 3), which suggests an important proportion of extremely fine particles (< 5 nm) of SP behavior.
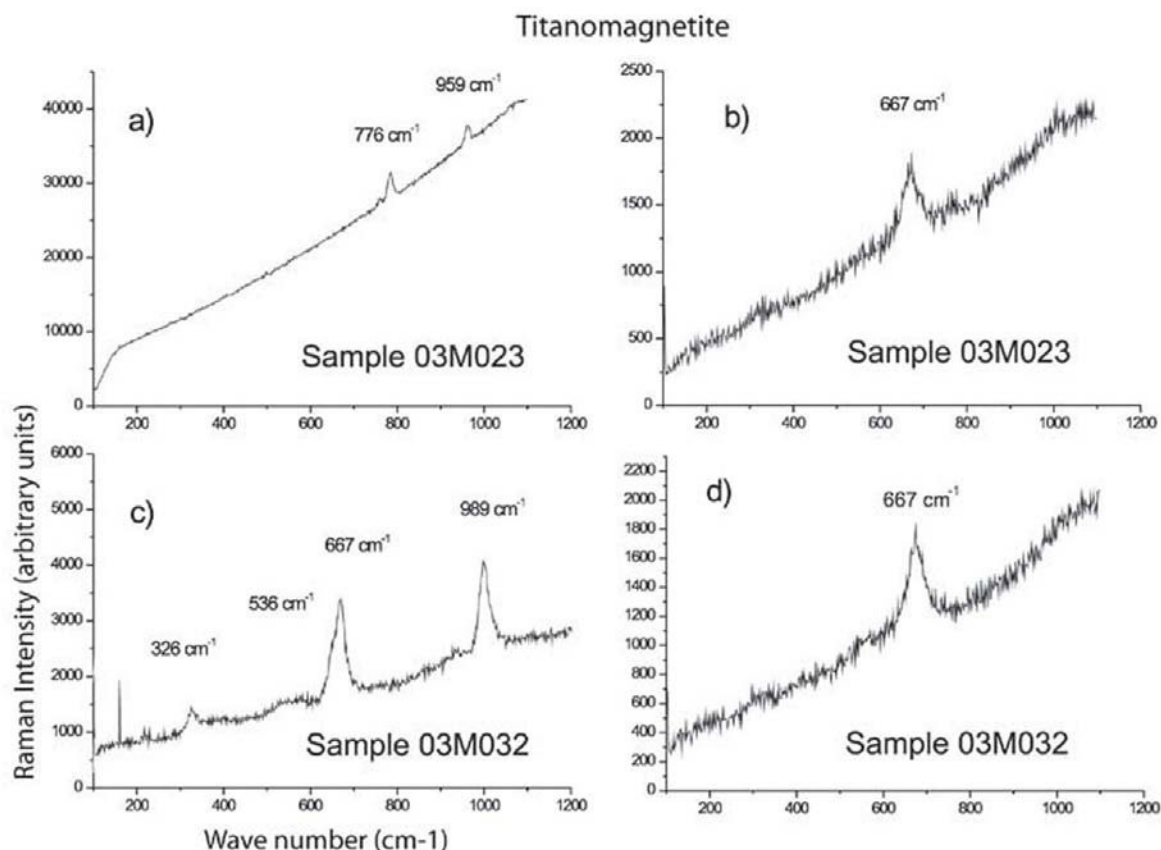
Figure 5. Raman spectra of selected regions pointing out to TM from pyroxenite Jacupiranga.

Rivas-Sánchez *et al*. (2009) reported similar values for samples with abundant magnetite nanoparticles included in berthierine: $\chi_{fd\%}$ = 3.4% in a magnetite sample constituted by 0.2 to 7 µm sizes, which are magnetite nanoparticles aggregates in a berthierine matrix. Corresponding Mössbauer spectroscopy for these samples indicate a 45.2% of SP particles, 44.8% for the ferromagnetic fraction, and a 10% of a paramagnetic fraction, of the total grain content. By association, these results support our conclusion about the SP dominant proportion grains in the sample of this study.

Magnetic susceptibility versus high temperature

Susceptibility vs. high temperature (*k-T*) experiments were carried out on the same samples described in Table 3. These magnetic concentrates (corresponding to TM with abundant ilmenite and TMf emulsion-type exsolutions) included samples

Figure 6. TMf nanostructure image obtained by high-resolution TEM (inset box shows the fast Fourier transform (FFT) analysis.
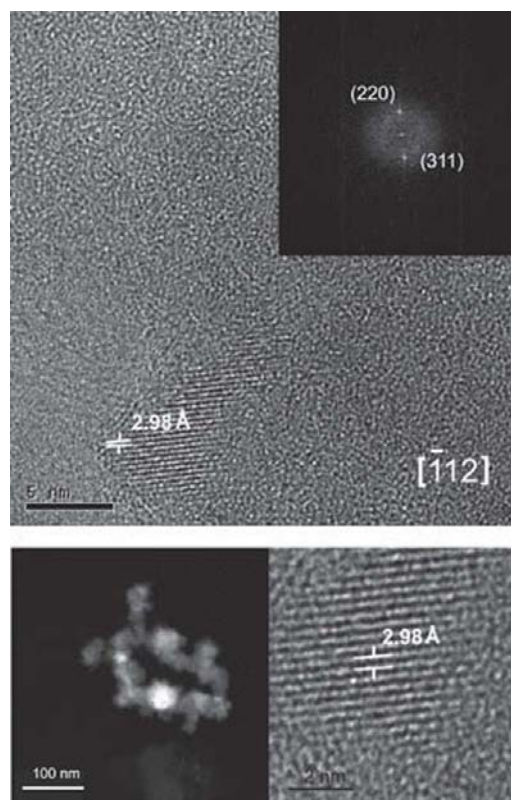
Table 3. Frequency dependent parameters and $\chi_{fd\%}$ of distinct magnetite grain size.

Sample	Size (µm)	Weight (g)	χ_{lf}	χ_{hf}	χ_{fd}	$\chi_{fd\%}$
MC_1	26 ± 2	1.1090	1018.03	991.88	0.025	2.57
MC_2	19 ± 1	0.7464	1158.89	1134.78	0.020	2.08
MC_3	13 ± 1	0.5068	1213.49	1156.27	0.047	4.71
MC_4	9 ± 1	0.5397	1013.53	972.76	0.040	4.02
MC_5	6 ± 1	0.6125	1182.04	1067.76	0.096	9.66
MC_6	6 ~ 0.1	0.6169	650.52	584.05	0.102	10.22

Figure 7. High-temperature k-T curves. Arrows indicate the heating/cooling curve. Experiments were done using magnetic concentrates of TM and TMf associated to ilmenite in agglomerated fractions of micrometric scale (a-g) and nanometric (h, i). The spectrum of (i) is the second run of the same heating as (h) in order to see the repeatability of this process during cooling phase.

in a size spectra from 45 to 9 μm show typical TM heating curves (soft Hopkinson peak and Curie temperature >550 °C) with slightly lower values on the cooling curves, effect of oxidation or partial transformation of TM to TMg (due to large amount of ilmenite and TMf exsolutions less than 1 μm size and inclusive at nanometer level). Dunlop and Özdemir (1997) describe that the multi-domain (MD) grains have a very soft Hopkinson peak, in comparison with those of single-domain (SD) grains. Accordingly, these curve types are typical for MD and SD grain sizes, considering that MD are > 2.0 μm and SD between 0.03 to 0.1 μm (Figure 7). Typical curves for minor grain size less than 6 μm (sample MC$_6$) shows a Hopkinson peak more conspicuous, related to a major content of < 1 μm particle size. In general, all curves show a delay during the oxidation from TM and TMf by temperature effect, with Curie temperatures higher that expected, 550 °C, the cooling curves are always lower than heating ones but the last two experiments, < 35 nm.

According to data presented in Table 2, magnesioferrite should be detectable in the *k-T* curves, which is not supported by the magnetic data because of the simple reason that our samples are magnetic TM concentrates. So, the least amount of magnetic minerals in these experiments obscures (mask) the possible response of the magnesioferrite.

Finally, two magnetic susceptibility versus temperature experiments of the same (< 35 nm) sample show that the repeatability during the second heating is probably due to the formation of new TMf nanoparticles and growth of those already present during the first heating process. Comparable results were reported by Rivas-Sánchez *et al*. (2009): 1) magnetite nanoparticles showed major resistance to heating; 2) formation of new magnetite nanoparticles; and 3) growing of those nanoparticles already present.

Hysteresis properties and isothermal remanent magnetization (IRM)

Hysteresis loop experiments obtained at room temperature at magnetic field strengths up to 1.5 T for the samples containing TM and magnesioferrite microparticles and range sizes described in Table 3 are shown in Figure 8. Table 4 shows a summary of the hysteresis parameters. The saturation remanent magnetization (Mrs), the saturation magnetization (Ms), and coercive force (Bc) were calculated after correction for the paramagnetic contribution. The coercivity of remanence (Bcr) was determined by applying progressively increasing backfield after saturation.

The general behavior of the hysteresis shaped loops like a ramp very close to the origin suggest TM, which is supported by the microscopic observations already described. These interpretations confirm the information coming from magnetic susceptibility experiments acquired with distinct frequencies that report high values of $\chi_{fd\%}$ for samples of particle size between 6 μm to 6-0.1 μm attributed to a dominant proportion of SP particles. It is remarkable that coercivity (Bc), in general, increase as the grain size decrease: from 26 μm, Bc= 14.6 mT up to Bc= 32.2 mT for sample size ranging from 6 to 0.1 μm. The Bcr/Bc ratio ranges from 1.784 to 1.590 and Mrs/Ms varies between 0.1491 and 0.2943 (Table 4). Rivas-Sánchez *et al*. (2009) obtained similar results by using agglomerates of magnetite nanostructures classified in micrometer sizes.

The hysteresis parameter plot indicates that all values fall in the PSD region (Figure 9). Day diagram (Day *et al*., 1977) shows a clear migration of the magnetization and coercivity ratios from PSD to SD, as grain size decreases.

Typical IRM acquisition curves for the TM – TMf of the same samples are shown in Figure 8 (inset).

Table 4. Hysteresis parameters.

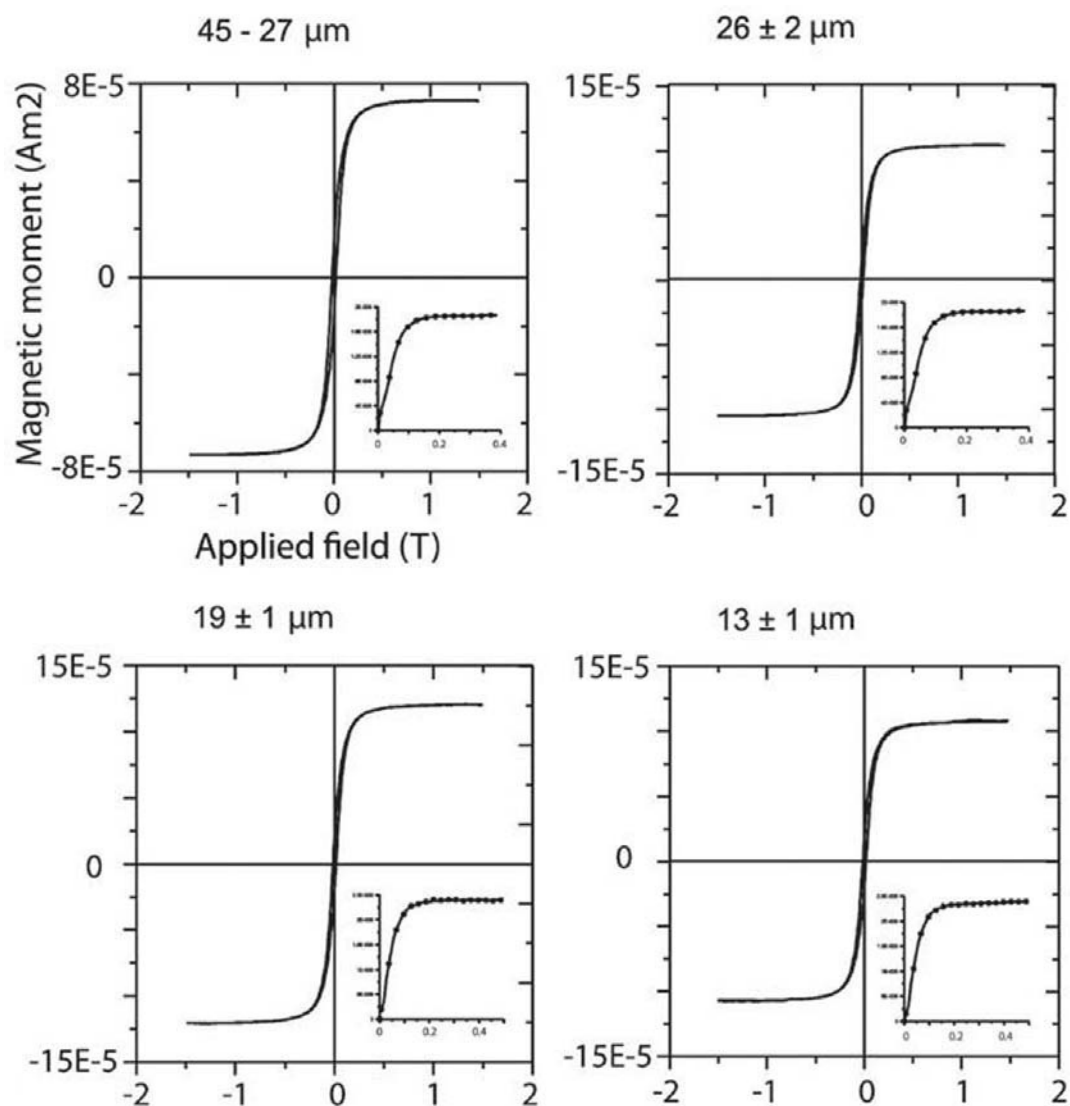| Sample	Mr (μAm²)	Ms (μAm²)	Mr/Ms	Hc (mT)	Hcr (mT)	Hcr/Hc	W (mg)	Ms/W (Am²/Kg)
26± 2 μm	15.60	104.6	0.1491	14.66	26.16	1.784	6.8	15.382
19± 1 μm	19.37	120.5	0.1607	15.42	25.54	1.656	12.0	10.041
13± 1 μm	19.16	107.7	0.1780	16.82	27.36	1.626	7.9	13.632
9± 1 μm	18.32	94.36	0.1941	18.39	29.94	1.628	6.4	14.743
6± 1 μm	25.87	118.6	0.2181	21.02	33.99	1.617	6.3	18.825
6~0.1μm	21.43	72.80	0.2943	32.20	51.22	1.590	12.6	5.777

W = weight

Figure 8. Hysteresis loops with paramagnetic correction for typical samples. Samples correspond to TM and TMf particles of distinct size ranges. Inset show isothermal remanent magnetization curves.

Figure 8. (Cont.)
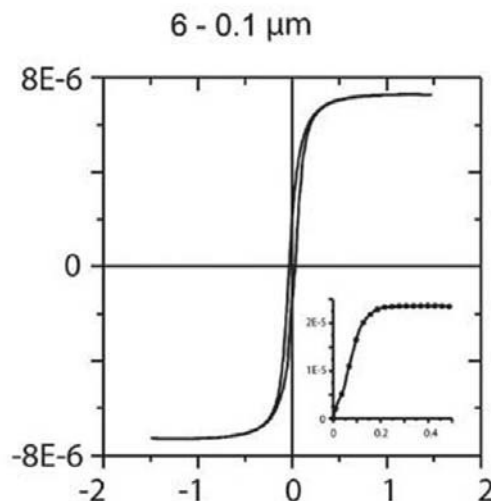
Major size samples show a rapid increase of the magnetization at low magnetic field and as the grain size decreases, a slightly larger magnetic field is required to get the saturation. The values to get this saturation are as follows: samples with sizes from 26 to 19 μm need 188 mT; samples ranging in size from 13 to 9 μm need 221 mT; and finally, samples with sizes lower than 6 μm require a magnetic field of 249 mT. All samples hold an important amount of SP particles. Rivas-Sánchez *et al*. (2009), conclude that the behaviour of magnetic properties is attributed to their atomic packing, textural arrangement, grains size, and that magnetite nanoparticle agglomeration requires that its magnetic domains display a distinctive behaviour in which SP properties and a major coercitive force require a major magnetic field intensity to reach saturation field.

Petrogenesis and metallogenesis

Alva-Valdivia *et al*. (2009) and Alva-Valdivia and López-Loera (2011) reported mineralogical and physical-chemical properties (host rocks and magnetic minerals). In this work, we did detailed observations of oxide minerals, their alteration minerals, mineralogical associations and textural relationships, which allow us to establish the paragenetic sequence of ultramafic rocks: a) In the carbonatite this is magnetite – magnesioferrite - geikielite; and b) In the pyroxenite this is TM – ilmenite – TMf – TMg – geikielite - TH. It is significant in this last sequence the roughly felted texture of the TM and its relation with micro- and nanometric scale TMf and ilmenite, which later were confirmed by high-resolution TEM observations.
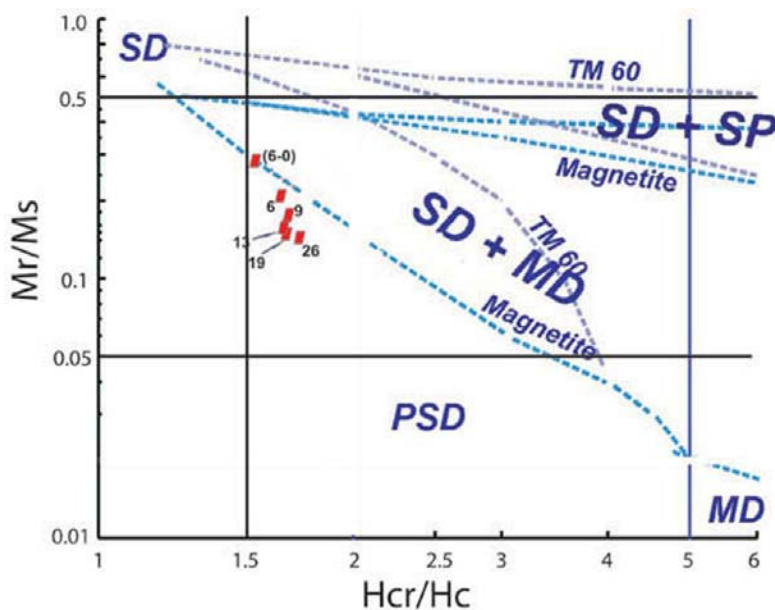
Figure 9. Day plot data for each fraction grain size (see numbers in microns).

The paragenetic sequence of the magnetic minerals in carbonatite and pyroxenite are distinctive of the magmatic and hydrothermal conditions during their formation, which is controlled by its crystallization-differentiation order, where the hydrothermal phase is the last one.

The chemical nature and structural formula of the magnetic mineralogy in carbonatite, shows 0 to < 2% TiO_2 content in the magnetite-magnesioferrite sequence, which is contrary to the magnetic mineralogy of the pyroxenite with TiO_2 >10% content suggesting the use of "titano" prefix to the magnetic mineral name of the pyroxenite.

The magnetic mineralization of carbonatite and pyroxenite are analogous mineralizations affected by partial substitution of Fe-ferrous by Mg. This type of ionic exchange was produced by circulation Mg-rich hydrothermal solution through porous and open spaces that substitute the Fe^{+2} of the magnetic mineralogy, making it Mg-rich. This process allowed that mineralization changed gradually from a magmatic body to high temperature hydrothermal, where Mg-rich magnetite and TM produced magnesioferrite and TMf in the carbonatite and pyroxenite, respectively.

The progressive change of primary mineralization is produced by a complex system of hydratation reactions and ionic exchange between the primary mineralization of the intrusive body and solutions, changing the composition of the hydrothermal fluid, its pH and the redox state (Tornos, 1997). The mineralization change gradually and its mineral chemistry and textural relations (size-shape) are affected drastically up to reach equilibrium. This progressive equilibrium process can explain the TMf, and possibly Fe-spinel and ilmenite nanoparticles formation. Ilmenite and Fe-spinel nanoparticles, in the pyroxenite, probably were formed during the last magmatic differentiation process.

We show quantitative results in terms of well-identified grain-size distribution that support the general theoretical basis of frequency-dependent magnetic susceptibility (Table 3) (Dearing *et al*., 1996). We observed the effect in natural TM comprising TMf particles with micro- to nanometer grain size.

Ti-magnetite and TMf particles ranging from 9 to 26 μm, provided low values for $\chi_{fd\%}$ < 5, probably due to the close association (amalgamation) of magnetic domains at micro-nanometer scale, where TM mask the SP signal of the TMf nanoparticles.

The results of a magnetic susceptibility vs. high temperature experiment of the < 35 nm of TM containing TMf nanoparticles sample produces a repetible curve (Figure 7 bottom right), which repeated in rapid succession suggest the probable formation of new TMf nanoparticles, which is similar to the results obtained by Rivas-Sánchez *et al*. (2009) and Hirt and Gehring (1991).

The first evidences of a hydrothermal process in carbonatite and pyroxenite are indicated by the next factors:

1. Texture (size-shape). In the carbonatite, magnetite is massive and surrounds the minerals forming the rock as apatite, forsterite, carbonates and phlogopite (Figure 10b, d, e, f), demonstrating its later crystallization to these forming minerals during the last magmatic differentiation phase that could be high-temperature hydrothermal. In the pyroxenite, TM formed afterwards showing a metasomatic texture with pyroxene grains (hedenbergite), evidencing the hydrothermal fluid reaction with the primary mineralization (TM with ilmenite exsolutions) of the intrusive rock previously consolidated. This event favored the TMf nanoparticle formation with Ti.

2. Fe^{+2} by Mg ionic exchange occurs in the metallic mineralization of carbonatite and pyroxenite. In the carbonatites, magnetite contains up to 4% of MgO and when this increase magnetite is transformed into magnesioferrite. In general, magnetite shows reaction borders when is in contact with dolomite (Figure 10e, f). The pyroxenite, TM and ilmenite exsolutions contain MgO, which remains constant from 3.5% and 9.5%, respectively, and TiO_2 is up to 10%. It is important to observe that in the carbonatite samples there are magnetite and magnesioferrite contained in some microareas with almost nothing Ti, contrary to the pyroxenite Jacupiranga samples.

3. Mineral chemistry. The TiO_2 content in the magnetite and magnesioferrite of the carbonatite is almost zero, in contrast with the TiO_2 of the TM and TMf of the pyroxenite that remains constant from 12% to 13%, as well as MgO in minor amounts to 3.5% and less that 1.7% of MnO (Table 1). The magnesioferrite contains more than 5% of MgO and few amounts of TiO_2 and MnO close to that of magnetite (Figure 11). Fe-mineralization of both rock types is replaced by geikielite along its borders and cross lines forming well developed parallel lamellas.

4. The paragenetic sequence of metallic mineralization of carbonatites and pyroxenites was inferred since the evidences showed above, which are closely related to their texture and mineral chemistry. So, we propose a hydrothermal effect in
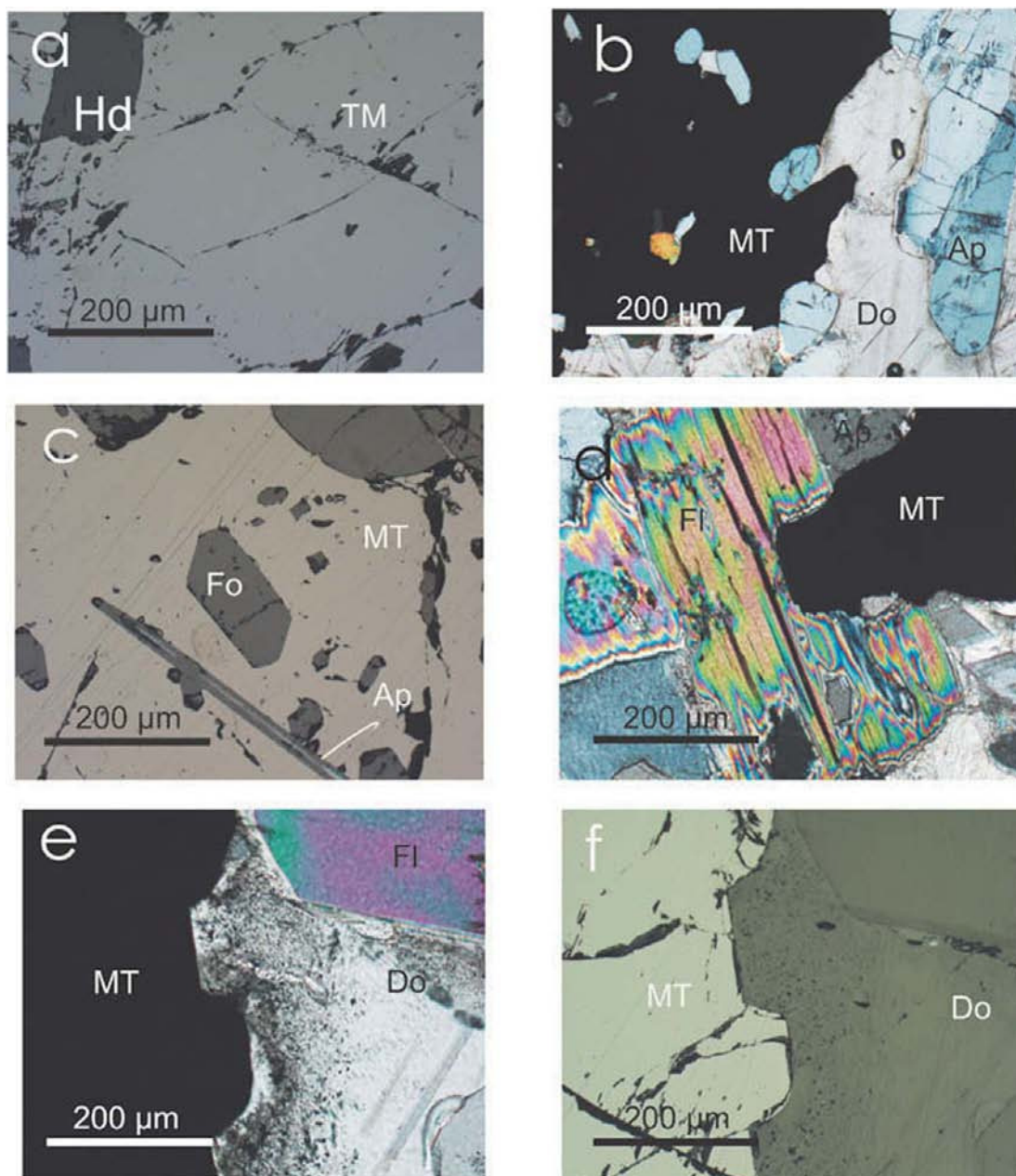
Figure 10. Optical microscope microphotographs of distinct textural aspects of massive Ti-magnetite (TM) in piroxenite and magnetite (M) in carbonatite with associated minerals: a) Massive Ti-magnetite with hedenbergite (Hd); b) Magnetite surrounding euhedral and subhedral crystal of apatite (Ap) and dolomite (Do); c) Forsterite (Fo) and apatite in the massive magnetite; d) Phlogopite sheet (Fl) cut by massive magnetite; and f) Massive magnetite in contact with dolomite, showing reaction borders and possible ionic exchange.

both rock types that occurred at the last magmatic differentiation phase. This process provoked metasomatism in the pyroxenite by reaction of the hydrothermal fluid with pyroxene intrusive massif that favored a chemical-mineralogical and textural change of the primary TM and ilmenite. All of this has an effect on its chemical composition that was enriched with Mg and its later partial transformation of the TM to TMf. It took also place a drastic change of its texture, forming TMf nanoparticles, and possibly spinel and ilmenite at nanometer scale. In the carbonatite, the hydrothermal process happened possibly at the same time that the formation of magnetite, enriched in Mg, forming the magnesioferrite. The geikielite was deposited later and replaced to the magnetite-magnesioferrite.
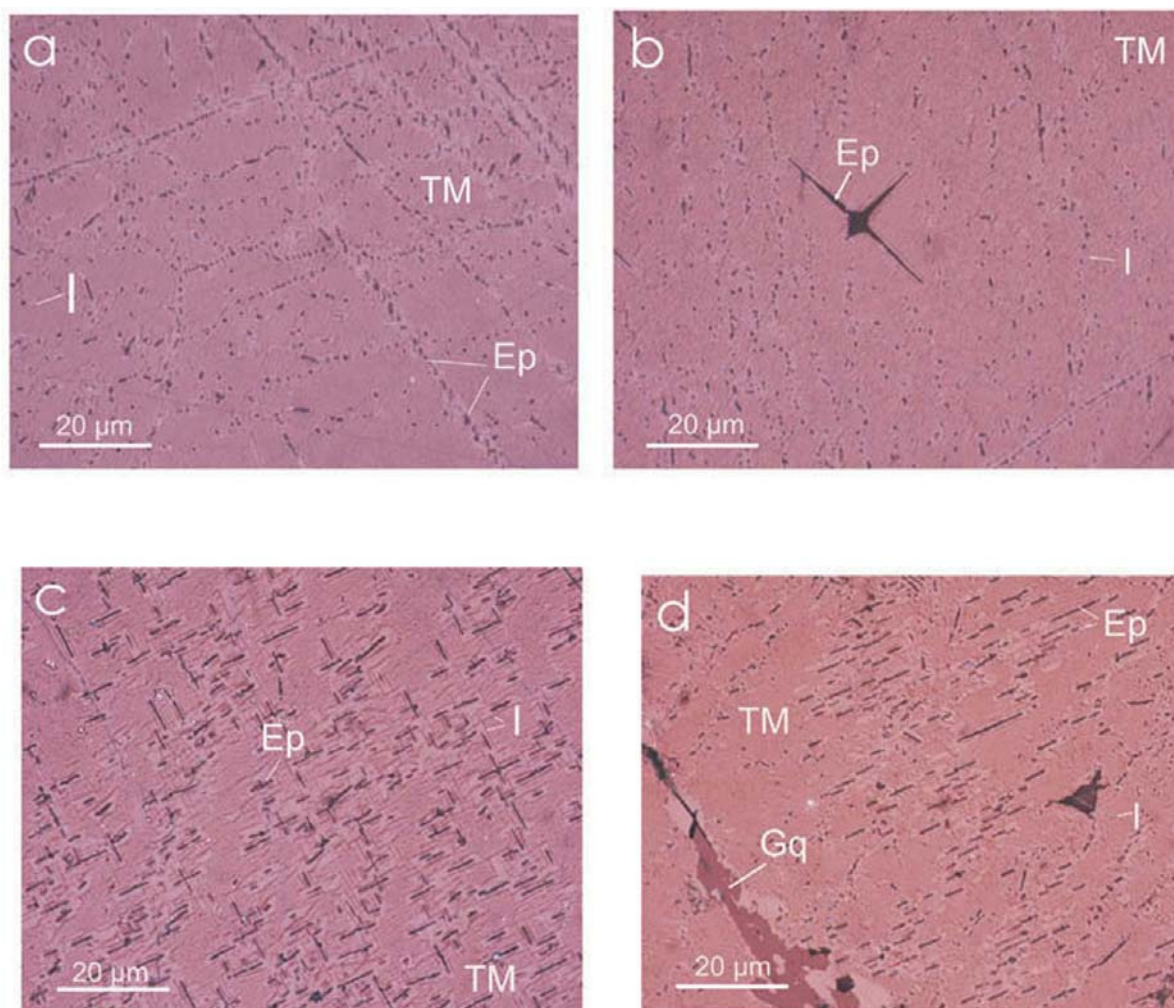
Figure 11. Optical microphotographs of metallic minerals in the pyroxenite: a-d) TM with abundant ilmenite (I) exsolutions and Fe spinel (Ep) homogeneously distributed.

Discussion

Our first results (Alva-Valdivia *et al*., 2009) show a complex mineralogy of the pyroxenite respect to the carbonatite that led to a detailed mineralogical study using magnetic concentrates of distinct grain sizes ranges. The magnetic concentrate is characterized by TM particles with TMf inclusions of nanometer and micrometer scale, ilmenite emulsion-type and Fe-spinel acicular exsolution. The ilmenite textural characteristics suggest that it is very probable to find it at nanometer scale. A minor proportion of TM particles are partly altered to TMg through the concave fractures and TH replacing TM along their cross lines forming trellis type texture associated to geikielite, pyroxene (hedenbergite-diopside) and apatite. An estimated proportion of metallic minerals of this sample is: TM, 51%; TMf, 22%; ilmenite, 6%; Fe spinel, 5%; Ti-magemite, 4% and Ti-hematite, 3%.

XRD analyses confirmed the existence of magnesioferrite and maghemite, their chemical composition and the structure formula: finding the TMf in our pyroxenite samples. Raman spectroscopy verified the ilmenite.

EPMA (using WDS) defined the chemical formula and structure of the complex Fe-Ti oxide minerals, being relevant for the Ti detection. We use the name of TM and TMf, for a structural formula of TiO_2 content up to 12% and 14%. The mentioned studies guide the selection of samples to perform the high-resolution TEM that identified the TMf nanoparticles of 5 to 10 nm size.

The magnetic concentrate is characterized by TM particles of less than 26 μm grain size, with TMf inclusions of nanometer and micrometer scale. The TM particles also have ilmenite emulsion-type and Fe spinel acicular exsolutions,

Mg (Al, Fe)$_2$O$_4$, both homogeneously distributed. Ilmenite textural characteristics suggest that it is very probable to find it at nanometer scale. An estimated proportion of metallic minerals of this sample is: TM, 51%; TMf, 32%; ilmenite, 10%; and Fe spinel 7%. Because of its chemical characteristics, we use the name of TMf, with a structural formula of Ti content up to 8%. The HRTEM study was performed using the magnetic concentrate of MC6 sample.

The rock magnetic properties of the Fe-Ti oxides ($\chi_{fd\%}$, k-T curves, hysteresis properties and IRM acquisition curves) support the finding of extremely fine particles (nanometer size) forming bigger (micrometer size) amalgamated particles. Sometimes, the rock magnetic signal are masked by stronger magnetic minerals (TM), making very difficult the definition of weaker magnetic TMf minerals.

We found by high resolution TEM that the TM and TMf form micrometer and nanometer crystalline structures, with specific and distinctive interplanar distances: for 3.00 Å and 2.56 Å TM, and 2.98 Å for TMf. The differences in grain size, represented by TM microparticles interacting with TMf nanostructures give rise to an interference in the ferromagnetic and SP signal, with the increase of the hysteresis parameters and important changes in the magnetization with decreasing of micrometer particle size.

Typical curve for k-T experiments of minor grain size less than 6 μm (sample MC$_6$) shows a Hopkinson peak more conspicuous, related to a major content of particles < 1 μm. In general, all curves show a delay during the oxidation from TM and magnesioferrite by temperature effect, with Curie temperatures higher that expected, 550 °C, the cooling curves are always lower than the heating ones excepting the last two experiments, < 35 μm.

These two magnetic susceptibility versus temperature experiments of the same (< 35 nm) sample show that the repeatability during the second heating is probably due to the formation of new TMf nanoparticles and growth of those already present during the first heating process. Similar results were reported by Rivas-Sánchez *et al*. (2009): magnetite nanoparticles showed major resistance to heating; and therefore to the new nanoparticle formation; and growing of those already existing during the k-T experiments.

The general behavior of the hysteresis curves is, like a ramp, very close to the origin.

The TM and TMf form micrometer and nanometer crystalline structures, with specific and distinctive interplanar distances: 3.00 Å and 2.56 Å for TM, and 2.98 Å for TMf, obtained by high resolution TEM. The differences in grain size, represented by TM microparticles interacting with TMf nanostructures provoke an interference in the ferromagnetic and SP signal, with the increase of the hysteresis parameters and important changes in the magnetization with decreasing of micrometer particle size.

Conclusions

This TMf particle study enabled to establish a better knowledge of their magnetic properties, mineralogical association and textural relationship (size-shape) with the TM. All of these information help to establish the paragenetic sequence and consequently the source of mineralization and deposition conditions.

The experience acquired during the progress of this work, demonstrate that TMf nanoparticles act like genetic guide regarding the environment conditions during their formation.

We identified TMf, and possibly spinel and ilmenite nanoparticles using the high-resolution TEM, which was supported by magnetic studies (magnetic susceptibility measured with distinct frequencies, magnetic susceptibility vs. high temperature curves, hysteresis analysis and IRM acquisition curves), and of course the mineralogical, chemical, mineral and textural relations of Fe-mineralization within carbonatite and pyroxenite. All of this supports the hypothesis of a high-temperature hydrothermal event during the final magmatic crystallization-differentiation process. This event affected the primary Fe-mineralization of the pyroxenite and at the same time of the carbonatite, producing the TMf in the pyroxenite by substitution of Fe^{+2} by Mg, as well as later deposition of geikielite and pyrite, pyrrhotite and marcasite.

Based on the mentioned magnetic properties, it was possible to choose sampling suggesting the presence of magnetic oxide nanoparticles, doing easier to look for the pursued nanoparticles by crystallographic and high-resolution TEM studies.

Acknowledgments

Bibliography

Alva-Valdivia L.M., Perrin M., Rivas-Sánchez M.L., Goguitchaichvili A., Lopez-Loera H., Ferreira Lopes O., Bastos Bonás T., 2009, Rock magnetism and microscopy of the Jacupiranga alkaline-carbonatitic complex, southern Brazil. *Earth Planets Space*, 61, 161–171.

Alva-Valdivia L.M., López-Loera H., 2011, A review of iron oxide transformations, rock magnetism and interpretation of magnetic anomalies: El Morro Mine (Brazil) a case study. *Geofísica Internacional,* 50, 341-362.

Day R., Fuller M., Schmidt V.A., 1977, Hysteresis properties of TMs: grain size and compositional dependence, Phys. *Earth Planet. Inter*., 13, 260–267.

Dearing J.A., Dann R.J.L., Hay K., Lees J.A., Loveland P.J., Maher B.A., O'Grady, 1996, Frequency-dependent susceptibility measurements of environmental materials, *Geophys. J. Int.*, 124, 228–240.

Dunlop D., Özdemir O., 1997, Rock-Magnetism, fundamentals and frontiers, Cambrige University Press, 573 pp.

Feinberg J.M., Harrison R.J., Kasama T., Simpson E.T., Dunin-Borkowski R.E., 2007, Electron Holography and Rock Magnetism: IRM Quarterly, 16, 4, p. 5.

Harrison R.J., 2007, The magnetic personality of minerals: from nano-scale microstructures to planetary-scale anomalies. Geol. Soc. Am. Denver Annual Meeting. Abstracts with Programs, 39, 6, p. 416.

Hirt A.M., Gehring A.U., 1991, Thermal Alteration of the Magnetic Mineralogy in Ferruginous Rocks. *J. Geophys. Res*., 96, B6, 9947–9953.

Hochella M.F., Jr., 2008, Nanogeoscience: From origins to cutting edge applications. *Elements,* 4, 373-378.

Hochella M.F. Jr., Lower S.K., Maurice P.A., Penn R.L., Sahai N., Sparks D.L., Twining B.S., 2008, Nanominerals, mineral nanoparticles, and Earth systems. *Science,* 319, 5870, 1631-1635, DOI: 10.1126/science.1141134.

McEnroe S.A., Skilbrei J.R., Robinson P., Heidelbach F., Lagenhorst F., Brown L.L., 2004, Magnetic anomalies, layered intrusions and Mars. *Geophys. Res. Let.,* 31, L19601, doi:10.1029/2004GL020640.

Rivas-Sánchez M.L., Alva-Valdivia L.M., Arenas-Alatorre J., Urrutia-Fucugauchi J., Perrin M., Goguitchaichvili A., Ruiz-Sandoval M., Ramos-Molina M.A., 2009, Natural magnetite nanoparticles from an iron-ore deposit: size dependence on magnetic properties, *Earth Planets Space,* 61**,** 151-160.

Ruberti E., Gomes C.B., Melchor G.C., 2000, The Jacupiranga Carbonatite Complex: geological and petrological aspects of the Jacupiranga alkaline-carbonatite association, southern Brazil, Post-Congress Field Trip Aft 08 Guidebook, International Geological Congress, Part I: 1–21, Rio de Janeiro, Brazil.

Tornos F., 1997, Procesos de alteracion y relleno hidrotermal sobre rocas silicoalumininicas, Atlas de asociaciones minerales en lamina delgada, Universidad de Barcelona, 249–271.